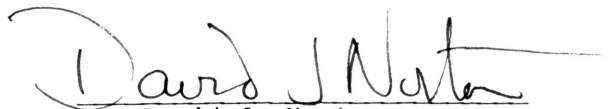WIND LOADS ON OFFSHORE STRUCTURES

by

Eddy Proft
Aerospace Engineering Department

Submitted in Partial Fulfillment of the Requirements of the
University Undergraduate Fellows Program

1978 - 1979

Approved by:

Dr. David J. Norton

April 1979

Abstract

A review of the state of the art of wind design procedures for off-shore structures indicated that wind/wave interactions were not taken into account. In hurricane conditions, large amplitude waves may cause cyclic loading on the platform due to the wind flowing between the waves and the platform deck. Also, the waves induce velocities which are not currently considered by designers when they formulate a design velocity profile. In order to model the problem a trochoidal wave with a 60 foot amplitude and 720 foot wavelength was chosen along with a 180' x 180' x 18' platform deck. Wind tunnel models were then built using a scale of 1:500. Velocity profiles above the waves were determined in both uniform and simulated atmospheric boundary layer approach flows. Lift forces on the model platform were then measured in the uniform flow. Experimental velocity perturbations were compared with a linear perturbation solution and a 4th order perturbation solution. It was concluded that the instantaneous velocity field above a wavy surface could be modeled as the sum of the reference velocity profile and the induced perturbation velocity profile with an increase in accuracy of up to 33% over current models. This could increase the accuracy of the dynamic pressure prediction by as much as 77% in the lower layers.

CONTENTS

SYMBOLS AND NOTATION

Primary Symbols

c	Dominant Wave Speed
C_D	Drag Coefficient
C_L	Lift Coefficient
F_D	Drag Force
F_L	Lift Force
n	Power Law Factor
q	Dynamic Pressure
s	Reference Area
u	X-Component of Velocity
$<u>$	Reference Velocity Profile
U_{rel}	Relative Velocity
$\tilde{u}$	Perturbation Velocity
U_∞	Free Stream Velocity
$u*$	Wall Friction Velocity
X	Horizontal Coordinate Measured from the Wave Crest
Z	Vertical Coordinate Measured From the Mean Water Line
Z_o	Roughness Length
δ	Boundry Layer Height
ε	Wave Amplitude
η	Scaled Vertical Coordinate
θ	Angle Swept Out by the Circle When Forming a Trochoid
λ	Wave Length
ξ	Scaled Horizontal Coordinate
ρ	Density

Subscripts

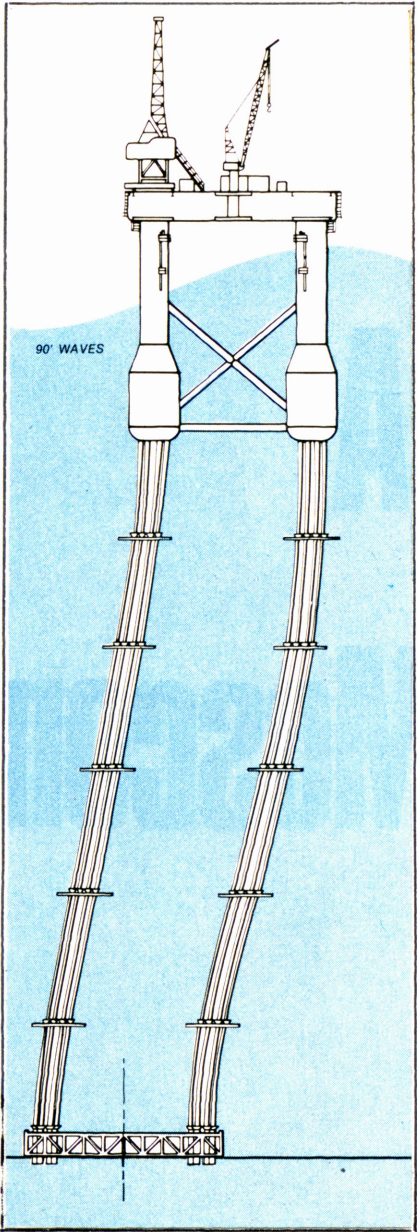|	
J.p.	Jenson Perturbation
s.p.	Small Purturbation
w	Wave

LIST OF FIGURES

Introduction:

As a result of the increased need for oil, offshore drilling platforms are being rapidly constructed to meet the demand. Figure (1) shows three typical offshore platforms. In view of the possibility of severe weather, problems arise which must be solved in order to insure safe and efficient operation of the rig. One problem which has arisen which has not been studied is the combined effect of wind and waves on drilling platforms. Current wind load design methods do not take into account the possibility of waves and their interaction with the wind. Such methods assume that the surface is fixed with distributed roughness and that the wind velocity over the surface can be modeled as either a uniform flow[1] or some type of marine atmospheric boundary layer[2]. The latter method typically uses a log law or power law to describe the boundary layer and is more descriptive of actual conditions than the uniform flow model in that it admits to the presence of viscous shearing stresses between the wind and water interface.

The research presented in this paper will be an attempt to determine by experimentation the wave induced velocities in both uniform and nonuniform (boundary layer) flow fields and the cyclic loading on the platform caused by the wind flowing between the waves and the platform deck. The experimental work will be supported by analytical modeling methods to develop an equation for the wind velocity profile that is more representative of hurricane conditions than the velocity profiles used currently by designers of offshore platforms.
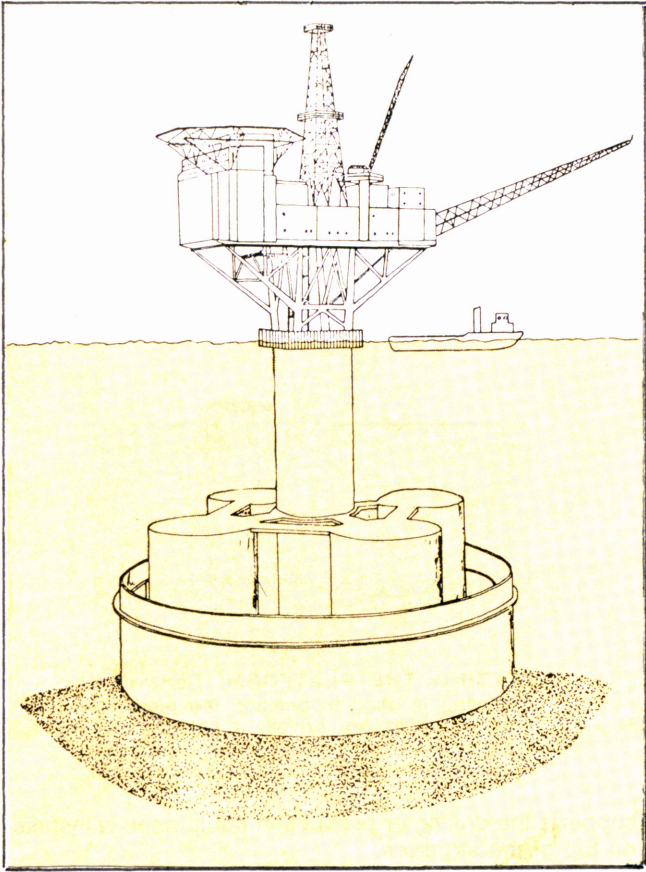
Concrete Platform

Jack-up Type Platform

Tension Leg Platform

Figure 1. Three Types of Offshore Platforms

Experimentation:

A wave experiment was set up to investigate the effects of simulated large amplitude waves on a velocity profile. A 2 x 3 ft. cross sectional area wind tunnel with a 5 ft. long test section was used throughout the experiment. A wave train consisting of three crests was constructed out of polystyrene at a scale of 1:500. From literature research it was determined that sinusoidal wave shapes were not representative of large amplitude waves. Since trochoidal waves have sharper crests and flatter troughs than those of sinusoidal waves and are considered to be more representative of large amplitude waves in the ocean[3], this shape was adopted. The surface of a trochoidal wave is described by:

$$x = \frac{\lambda}{2\pi} \theta + \varepsilon \sin\theta \tag{1}$$

$$z = \varepsilon \cos\theta \tag{2}$$

For the design wave used, ε = 30 ft. and λ = 720 ft.

Velocity profiles above the wave were measured at seven different stations from one crest to the next by use of a hot-wire anemometer. Figure (2) shows a trochoidal wave shape with the experimental stations labeled. A linearized hot-wire anemometer was traversed vertically from the wave surface to determine velocity profiles near the wave surface. These velocity profiles were plotted automatically on an x-y plotter for latter analysis.

The first phases of the experiment involved measuring the velocity profiles above the wave in an initially uniform flow field having a constant velocity of 65.6 ft/sec. A turbulence grid was placed at the entrance to the test section after flow visualizaton techniques indicated
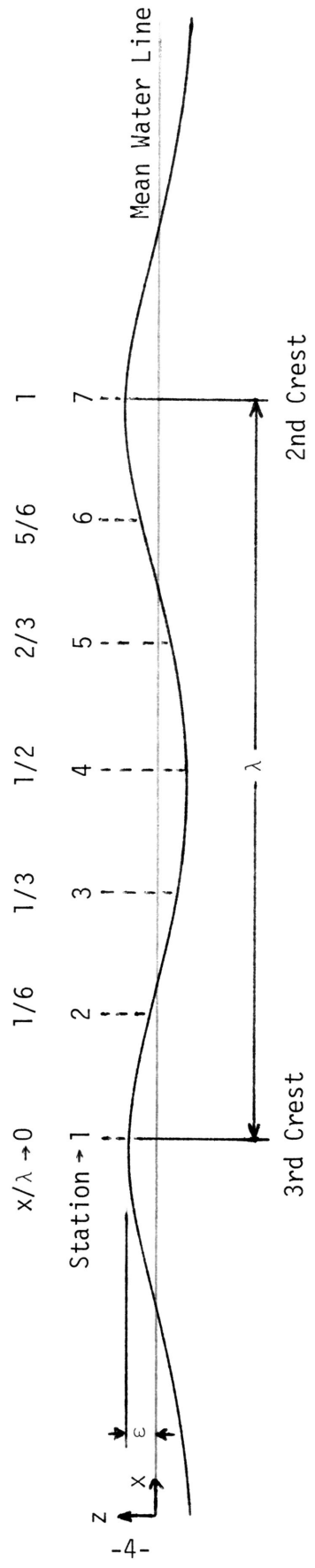
Figure 2. Trochoidal Wave Shape Showing the Locations of the Experimental Stations

that the flow was separating just downstream from the crest and reattaching at mid-trough. The grid produced freestream turbulence of 8% which created a turbulent boundary layer and therefore allowed the flow to remain attached. The measured velocity profiles for this case are shown in Figure (3).

In the second phase of the experiment, the velocity profiles above the wave were measured in an initial simulated atmospheric boundary layer velocity profile. Studies indicate that the average atmospheric boundary layer extends to a height of about 1000 ft. above the earth's surface[4]. Using the scale of 1:500, the simulated boundary layer had a height of 2 ft. and therefore encompassed the entire entrance to the test section. In modeling the initial boundary layer velocity profile, a power law was used, which is common practive among design engineers. The power law equation is :

$$\left(\frac{u}{U_\infty}\right) = \left(\frac{z}{\delta}\right)^{1/n} \tag{3}$$

where, δ is the boundary layer height and n the power law factor.

It was desirable to simulate a 1/7th power law boundary layer velocity profile in the wind tunnel. To do this, boundary layer spires were placed at the entrance to the test section. Since there is no analytical method for designing spires, many different shapes were tested. The final shape and layout of the spires used is shown in Figure (4). The velocity profile produced by these spires is compared to that of a 1/7th power law in Figure (5). In an attempt to better fit the experimental data, an average power law factor was computed using:
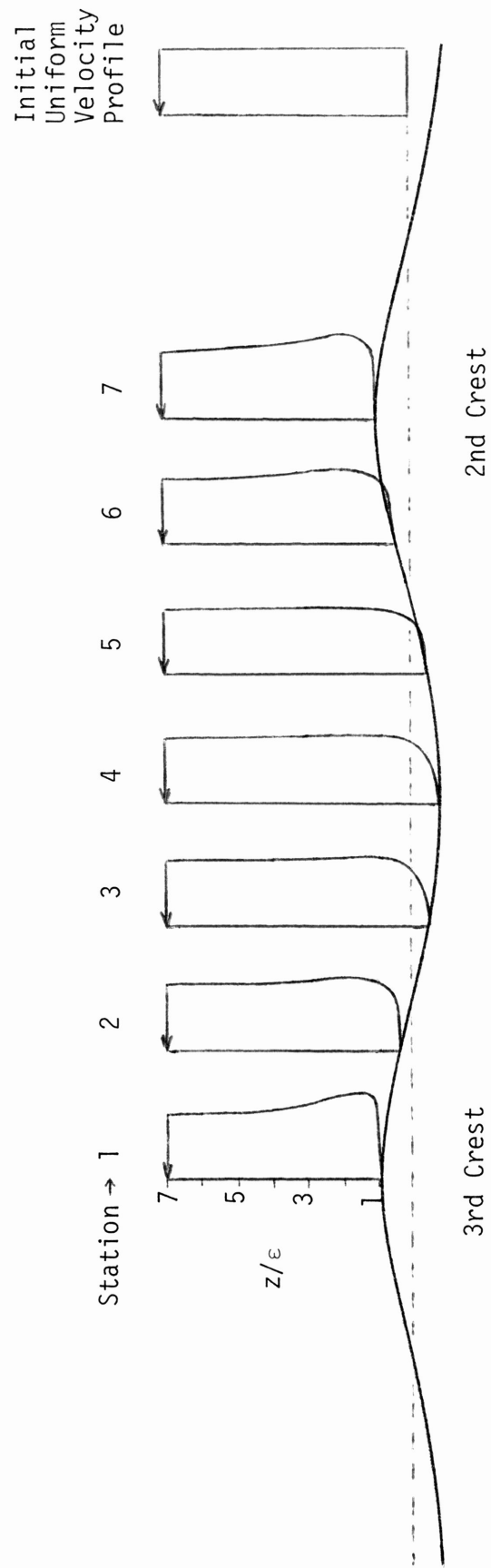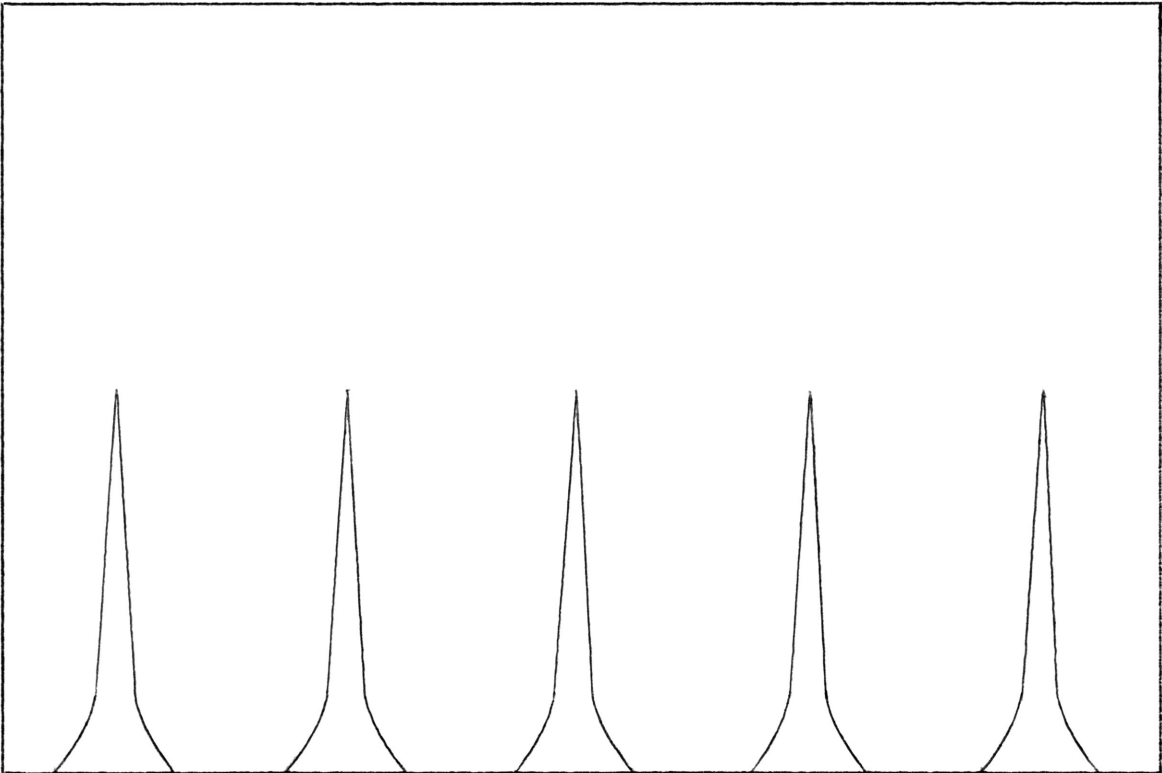
Figure 3. Measured Velocity Profiles in an Initially Uniform Flow Field

Test Section Entrance
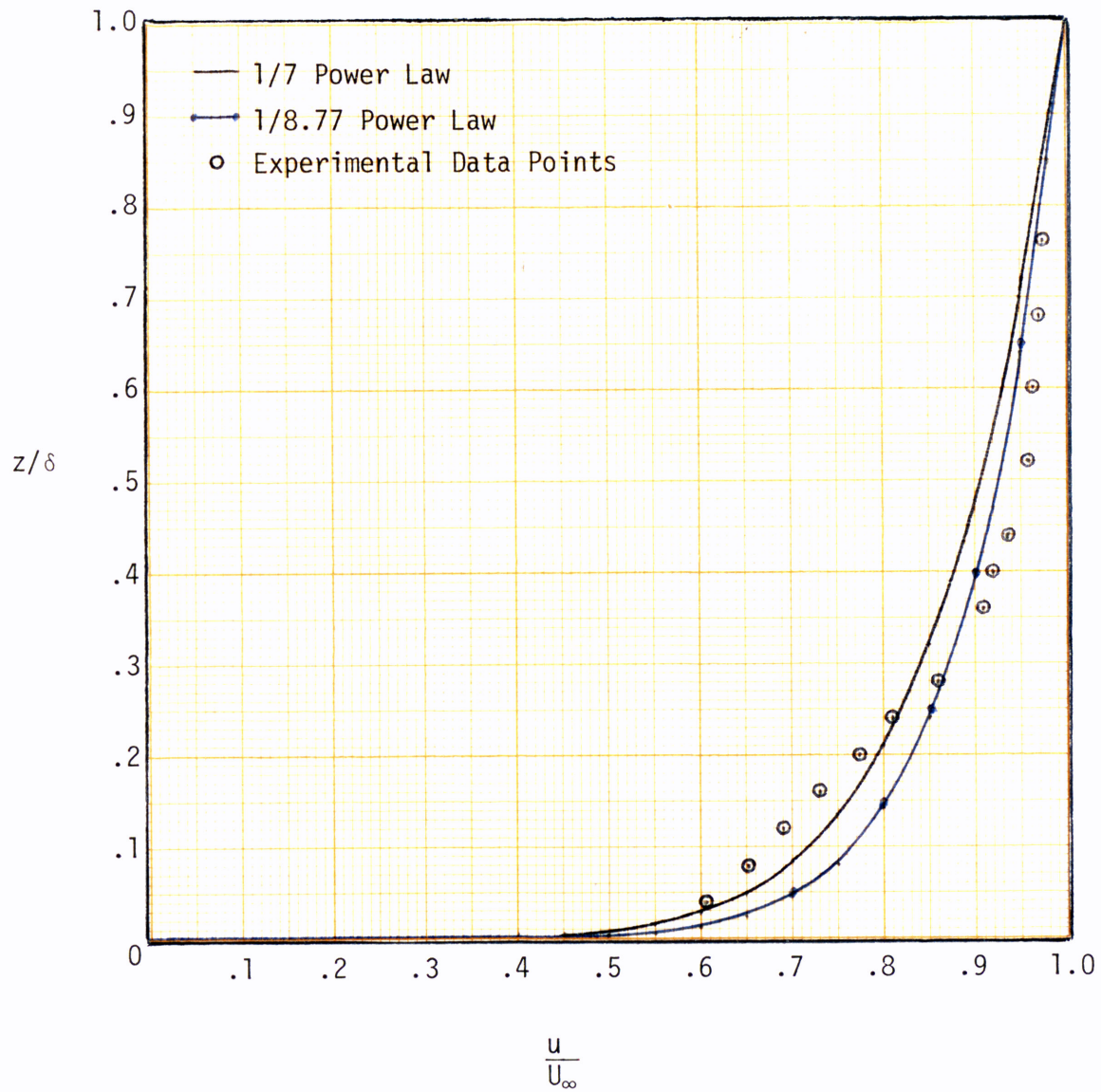
Figure 4. Boundary Layer Spires

Figure 5. Boundary Layer Velocity Profile Comparisons

$$n = \frac{1}{\frac{1}{N} \sum\limits_{i=1}^{N} \frac{\ln(\frac{u}{U_\infty})_i}{\ln(\frac{z}{\delta})_i}} = \frac{1}{8.77} \tag{4}$$

where N equals the number of data points. The velocity profile using the above value for n is also plotted in Figure (5). With the boundary layer spires in place and the turbulence grid removed, the velocity profiles above the wave were measured. The results are shown in Figure (6).

In the final phase of the experiment, the effects of the wave induced perturbation velocities on a simulated platform deck were investigated. A model was constructed out of thin brass plates at a scale of 1:500. It was 1/4 of the model wave length and had the dimensions of 4.32 in. in length and width and .432 in. in thickness. There were 20 pressure orifices on one surface of the model which were read through a scanivalve. The model was sting mounted and constructed in a manner whereby it could be inverted to obtain pressures on both the top and the bottom. This made it possible to integrate the pressure distribution to determine the lift coefficient, C_L. The sting was connected to a traversing mechanism making it possible to vary the height of the model platform above the wave's surface. The experimental setup is shown in Figure (7).

The model platform was traversed at the seven stations on the wave in the initially uniform flow field case. Figure (8) shows the results of these experiments. Notice that as the height above the wave crest, z/ϵ, is increased, the C_L tends toward zero. This indicates a return to more uniform flow as z/ϵ becomes large. The results also show that a large cyclical variation in lift force may be expected as the waves pass beneath the deck. Very close to the wave crest viscous effects allow a stagnation pressure to develop beneath the platform, however as λ/ϵ
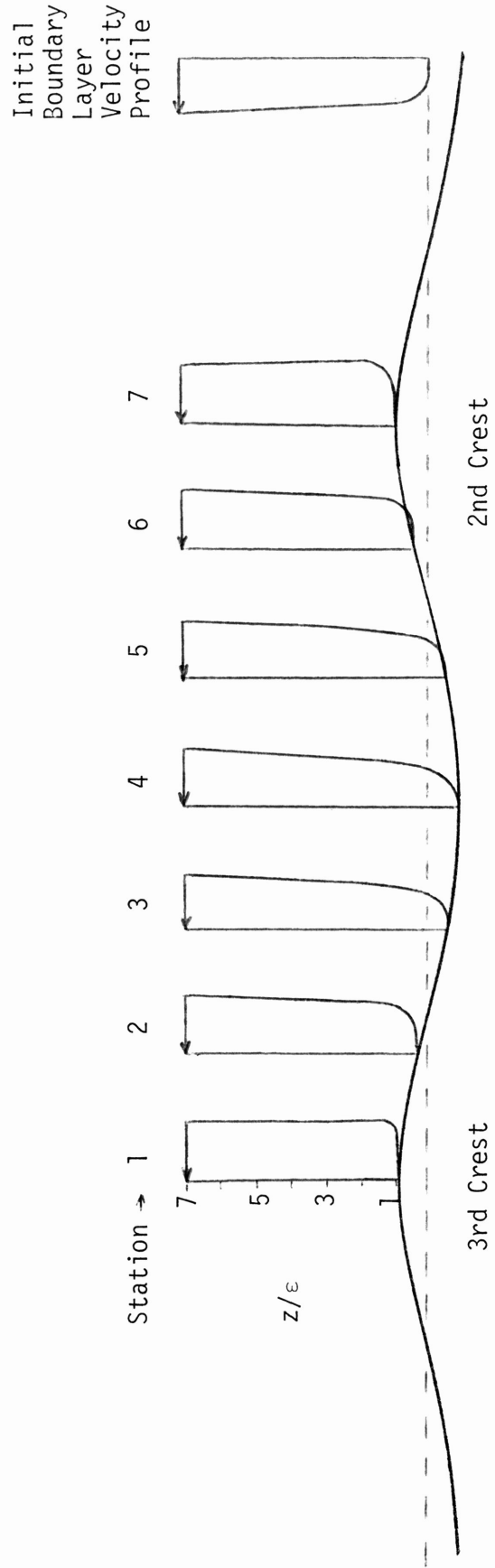
Figure 6. Measured Velocity Profiles in an Initial Boundary Layer Flow Field
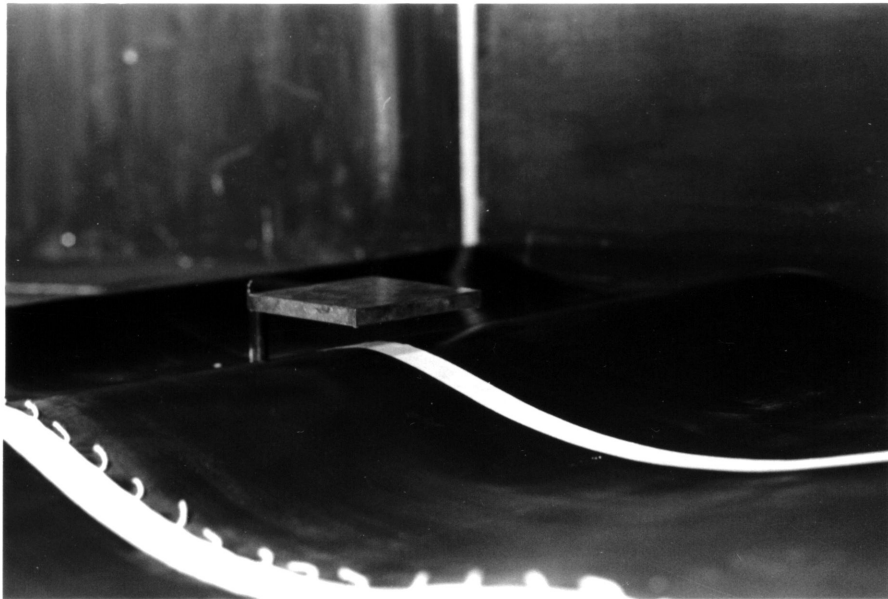
-10-

Figure 7. Experimental Set-up of the Platform and Waves
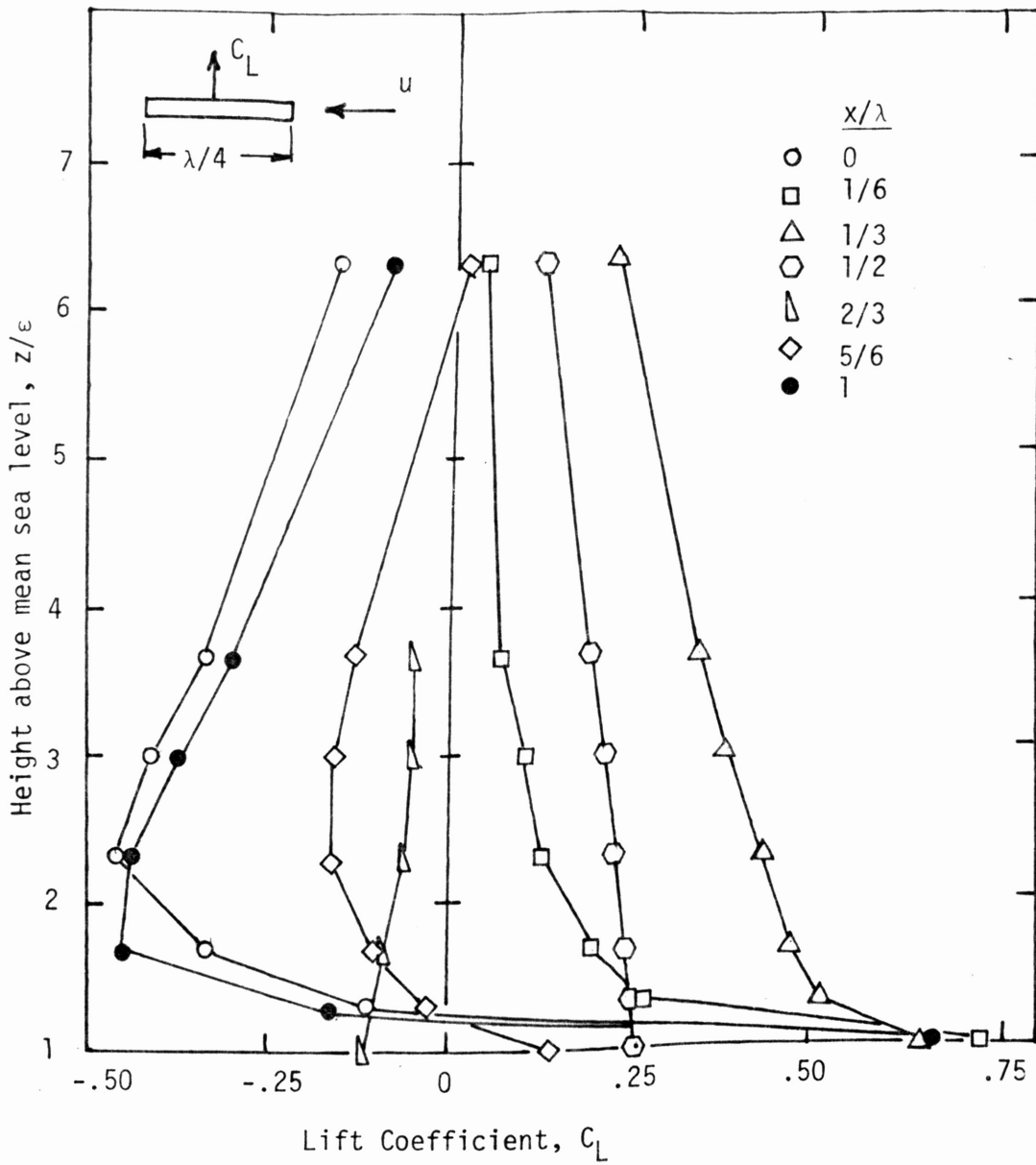
Figure 8. Measured Lift Coefficients Acting on the Platform

increases this changes to a venturi effect which produces a suction.

Theory:

The instantaneous velocity field, u, above a wavy surface can be viewed as having two components: the reference wind profile, $<u>$; and the wave induced perturbation velocity, $\tilde{u}$.

$$u = <u> + \tilde{u} \tag{5}$$

Three ways in which to model the reference wind profile are shown below.

1. $<u> = U_\infty = $ constant with altitude $\tag{6}$

2. $<u> = U_\infty \left(\frac{z}{\delta}\right)^{1/n}$ - power law $\tag{7}$

3. $<u> = \frac{u^*}{k} \ln\left(\frac{z}{z_0}\right)$ - log law $\tag{8}$

The first model would be indicative of a uniform flow field whereas the latter two would indicate boundary layer velocity profiles.

The wave induced perturbation velocity was initially modeled using linear, or small, perturbation theory for the flow over a cosinusoidal wavy wall[5]. The assumptions of small perturbation theory are:

1. $\frac{2\pi\varepsilon}{\lambda} << 1$

$\tag{9}$

2. $\frac{\tilde{u}}{U_\infty} << 1$

3. The boundary conditions are applied at $z = 0$.

4. Irrotational flow

5. Inviscid flow

It can be shown that large amplitude waves such as the model wave produce ratios of $2\pi\varepsilon/\lambda$ in the neighborhood of 1/4. Ratios of this size are normally out of the accuracy range for small perturbation and lead to difficulty in determining the velocity at the wave surface since $z \not\cong 0$. Also, the model wave was trochoidal in shape and not cosinusoidal. Nevertheless, as a first approximation, small perturbation theory was used. For a wave defined by the function

-14-

$$z = -\varepsilon \cos\left(\frac{2\pi x}{\lambda}\right) \tag{10}$$

the perturbation velocity is

$$\tilde{u} = -(U_{rel}) \frac{2\pi\varepsilon}{\lambda} \cos\left(\frac{2\pi x}{\lambda}\right) e^{-\frac{2\pi z}{\lambda}} \tag{11}$$

where, U_{rel} is the relative velocity between the free stream and the wave. This indicates that the perturbation velocity is greatest at the crest and the trough and dies out exponentially with height above the wave. When the waves are propagating in the same direction as the wind, $U_{rel}=U_\infty-c$. Therefore, the nondimensionalized small perturbation equation is:

$$\frac{\tilde{u}}{U_\infty} = \left(1 - \frac{c}{U_\infty}\right) f(x,z)_{s.p.} \tag{12}$$

where, $f(x,z)_{s.p.} = -\frac{2\pi\varepsilon}{\lambda} \cos\left(\frac{2\pi x}{\lambda}\right) e^{-\frac{2\pi z}{\lambda}}$ and represents the nondimensionalized perturbation. As is expected, no perturbation results when the free stream wind velocity equals that of the wave.

The small perturbation equation is but the linear part of a more general equation. To account for large amplitude waves and various wave shapes, higher order terms must be added. One such equation which takes into account the above is Jenson's 4th order perturbation equation for flow over a trochoidal wave shape. This equation was derived by Dr. Jenson at Texas A&M[6]. The derivation of his equation will not be presented herein, only the final result. Though the ratio $\frac{2\pi\varepsilon}{\lambda}$ does not have to be small in the same sense as the linear approximation, the assumptions of irrotational flow and the boundary conditions being applied at z=0 are still true. Jenson's equation for the nondimensionalized perturbation velocity in the x direction is

$$\frac{\tilde{u}(\xi,\eta)}{U_\infty} = \left(1-\frac{c}{U_\infty}\right) \left[-e^{\eta}\cos(\xi) + 2e^{2\eta}\cos(2\xi) - \frac{9}{2}\cos(3\xi)\,e^{3\eta} + \right.$$

$$\left. \frac{32}{3}\,e^{4\eta}\cos(4\xi)\right] \tag{13}$$

-15-

where, $\xi = \dfrac{2\pi x}{\lambda}$

$\eta = \dfrac{-2\pi}{\lambda} z + \ln(\dfrac{2\pi\varepsilon}{\lambda})$ (14)

Notice that the first term in the brackets, in eqn. (13) is the linear, or small, perturbation portion. The perturbation velocity can also be represented as

$$\dfrac{\tilde{u}}{U_\infty} = (1 - \dfrac{C}{U_\infty})\ f(x,z)_{J.p.} \qquad (15)$$

where, $f(x,z)_{J.p.}$ is the bracketed terms or, as before, the nondimensionalized perturbation.

Therefore, the final form of the instantaneous nondimensionalized velocity field above a wavy surface is

$$\dfrac{u}{U_\infty} = \dfrac{<u>}{U_\infty} + (1 - \dfrac{C}{U_\infty})\ f(x,z) \qquad (16)$$

where $f(x,z) = f(x,z)_{s.p.}$ or $f(x,z)_{J.p.}$

RESULTS

Since the waves were not moving in the wind tunnel, c=0 and the
nondimensionalized equation for the velocity field reduces to:

$$\frac{u}{U_\infty} = \frac{<u>}{U_\infty} + f(x,z) \tag{17}$$

The nondimensionalized perturbation part of this equation is now just

$$\frac{\tilde{u}}{U_\infty} = f(x,z) \tag{18}$$

Since only the x-component, u, of the perturbation velocity is present on the
crest or in the trough, comparisons of theory and experimental data were
made only on these two locations.

The perturbation velocities over a trochoidal wave crest are shown in
Figure (9). As can be seen, Jenson's perturbation equation agrees better
with the experimental data than does the linear perturbation equation.
The dashed lines extending from the two theoretical solutions show how
perturbation theory breaks down when the boundary conditions are applied
at $z/\varepsilon=0$. Notice also that a maximum perturbation of 33% from the free-
stream is reached. Figure (10) shows the perturbation velocities over a
wave trough. In this case, Jenson's perturbation theory predicts a
smaller pertrubation than does the linear perturbation theory. This is
due to the fact that Jenson's theory takes into account the flatness of
the trough. Neither of the theories, however, agree very closely with
the experimental results. This disagreement can be attributed to the
fact that the trough appears to be flatter than predicted because of the
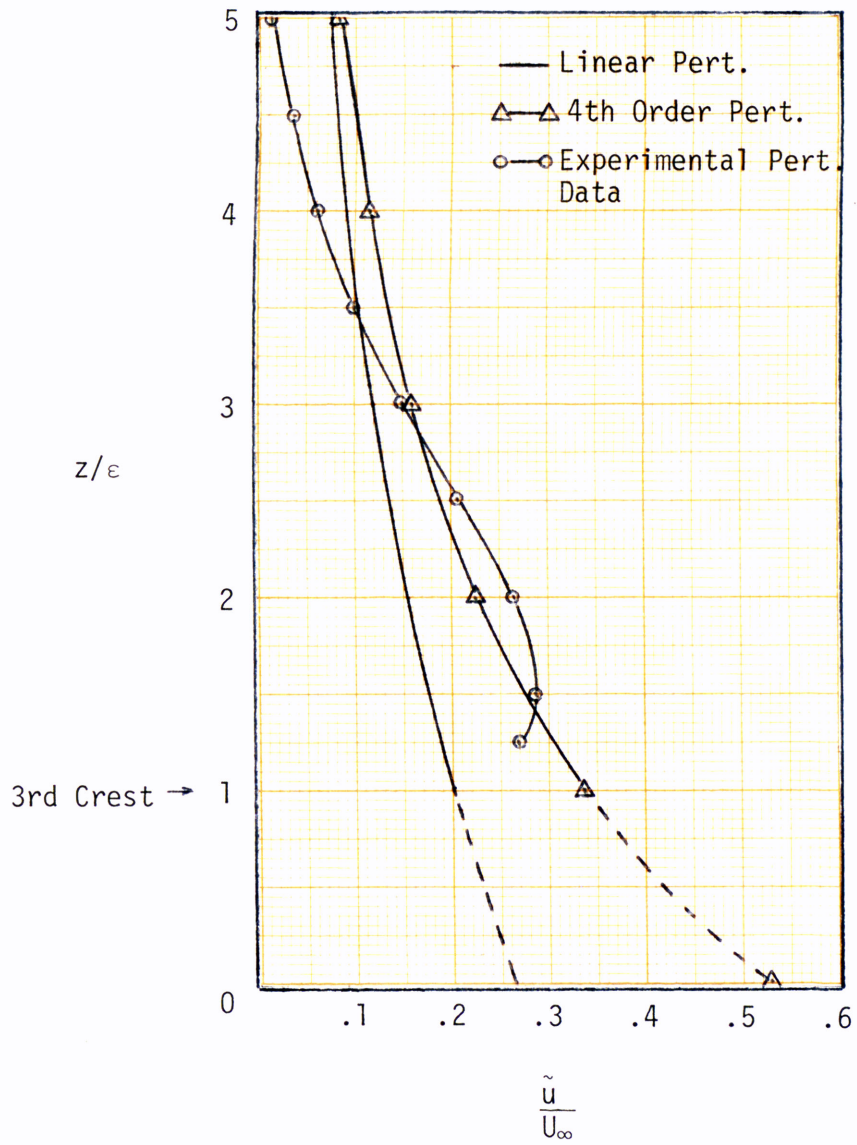thickening of the local boundary layer. Also, the assumption of

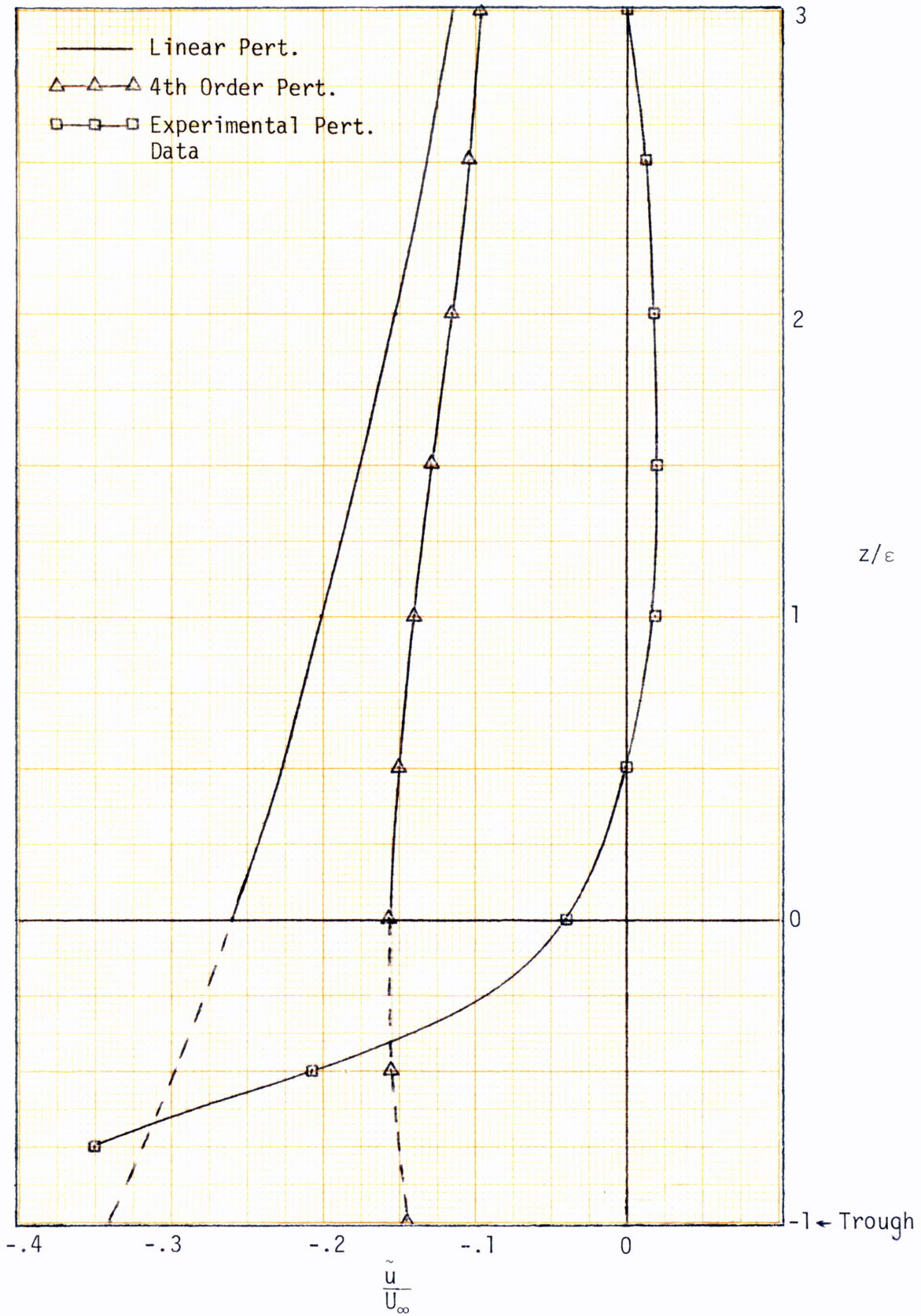Figure 9.   Perturbation Velocities Over a Trochoidal Wave Crest

Figure 10. Perturbation Velocities in a Trochoidal Wave Trough

-19-

irrotational, inviscid flow is suspect at the lowest layers.

Since the existance of an atmospheric boundary layer is more realistic than that of a uniform velocity profile, the latter will not be considered further. Instead, the power law will be used to represent the atmospheric boundary layer. For the experimental case,

$$<u>/U_\infty = [(z/\epsilon)/(\delta/\epsilon)]^{1/8.77} = [(z/\epsilon)/31.03]^{1/8.77} \tag{19}$$

At this point, the assumption was made that the reference atmospheric boundary layer "floats" along the wave, that is, it follows the contour of the wave without changing shape. This assumption allows the reference wind profile to go to zero at the surface of the wave. With this assumption, the following equation for the nondimensionalized reference wind profile results in

$$<u>/U_\infty = [(z/\epsilon - z_w/\epsilon)/31.03]^{1/8.77} \tag{20}$$

The instantaneous velocity field is now given by,

$$u/U_\infty = [(z/\epsilon - z_w/\epsilon)/31.03]^{1/8.77} + f(x,z)_{J.p.} \tag{21}$$

Comparison of this equation with experimental data is shown in Figure (11). Very good agreement is shown at the crest. Agreement is not good in the trough due to the reasons cited previously. Notice also that the theoretical perturbed velocities do not go to zero at the surface. This is due to the assumption of inviscid flow for the perturbation. Since the crest produces the larger and therefore more critical perturbations, it will be the area of primary concern. It can be concluded then that the proposed model for the instantaneous velocity field above a wave surface can be used by designers of offshore platforms with as much as 33% greater
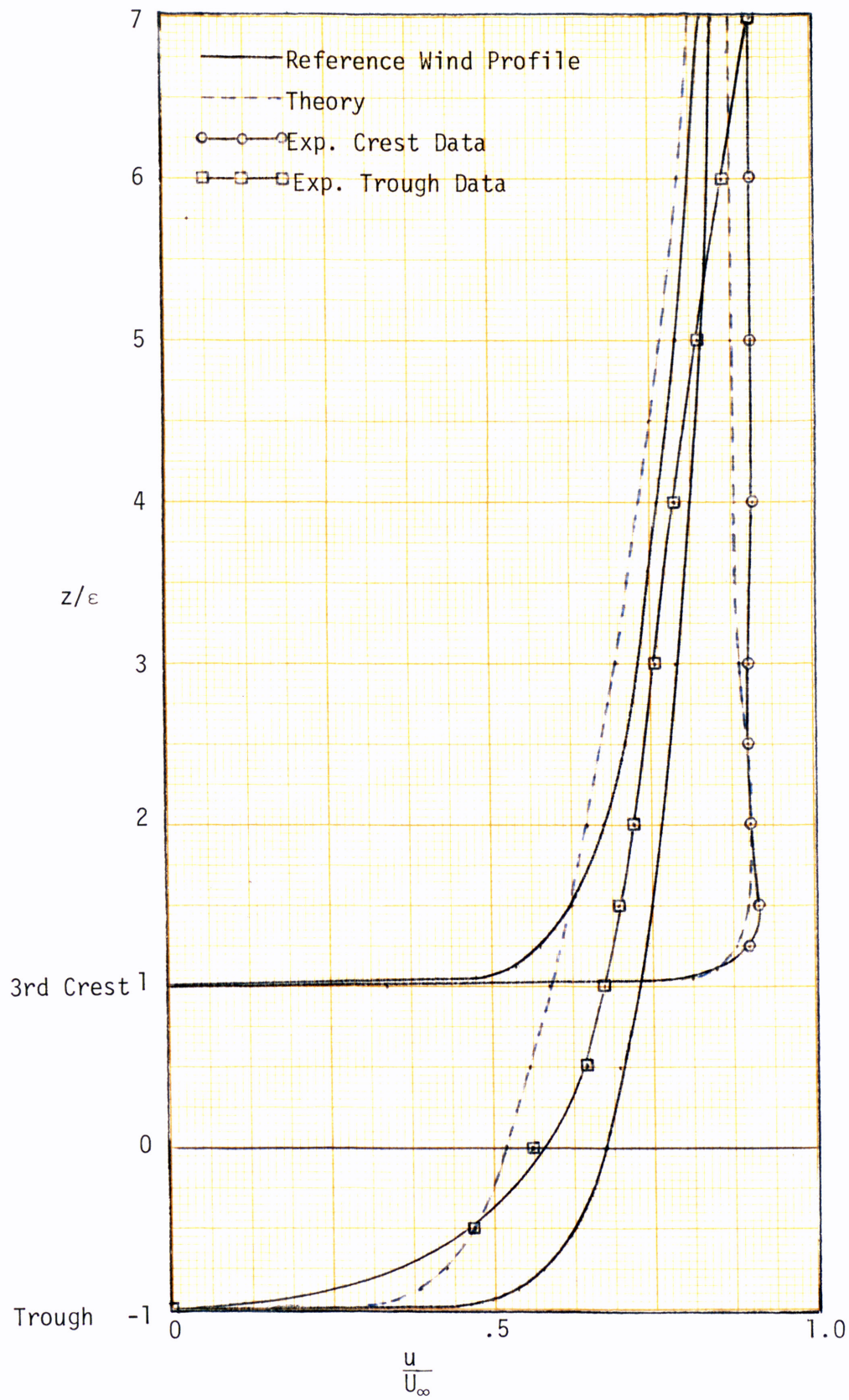
-20-

Figure 11. Theoretical and Experimental Velocity Profiles Over a Trochoidal Wave

accuracy than in the past.

The dynamic pressure of the wind is given by: $q = \rho u^2/2$
Using the proposed model for u yields

$$q(x,z) = \rho(<u> + \tilde{u})^2/2 \qquad (22)$$

This is a funciton of wave shape, c, U_∞, the wind profile, ε/λ, etc.
Therefore, q is no longer a constant. Since the velocity profile can be
corrected by as much as 33% this implies that the dynamic pressure can be
corrected by as much as 77%. The lift and drag forces on the platform
can be found from the following equations

$$F_L = q(x,z) \, S \, C_D \qquad (23)$$

$$F_D = q(x,z) \, S \, C_L \qquad (24)$$

where, S is some reference area. Also, the coefficient of drag, C_D, will
be approximately constant whereas C_L, as shown in Figure (8), will not be.

CONCLUSIONS

The purpose of this study was to investigate the combined effects of wind and waves on offshore drilling platforms. The objectives were: (1) to investigate the cyclic loading on a platform deck due to the oscillating component of the wind induced by the passage of large amptitude waves; and (2) to develop an equation for the wind velocity profile that is more representative of actual conditions than the velocity profiles used currently by designers. Based on the results obtained, several conclusions can be made.

(1) The cyclic loading on a platform decreases as the platform is moved away from the waves.

(2) The proposed model for the instantaneous wind speed above a wavy surface can be used with up to 33% more accuracy than models used currently.

(3) The dynamic pressure of the wind can be determined using the proposed model with an increase in accuracy of 77%.

ACKNOWLEDGEMENTS

REFERENCES

1. American Petroleum Institute, "Planning, Designing, and Constructing Fixed Offshore Platforms", API-RP-2A, 8th edition, Washington, D.C. April 1977.

2. American National Standards Institute, "Building Code Requirements for Minimum Design Loads in Buildings and Other Structures", ANSI A58.1, New York, New York, July 1972

3. Russell, R. C. and McMillan, D. H., Waves and Tides, Second Edition Greycaines, Watford, 1954, p. 41.

4. Simiu, E. and Scanlan, R. H., Wind Effects on Structures, John Wiley and Sons, New York, 1978 pp 36-71.

5. Eiepman, H. W., and Roshko, A., Elements of Gas Dynamics, John Wiley and Sons N.Y. 1953, pp 208-212.

6. Jenson, R. Personal Communication, March 1979.